Shock Capturing Numerical Method for Calculating Supersonic Flows

F. WALKDEN,* G. T. LAWS,† AND P. CAINE‡
University of Salford, Salford, Lancashire, England

A first-order method for predicting three-dimensional steady flow past aerodynamic shapes is described. Finite-difference equations which smooth real shock discontinuities are derived from a semicharacteristic representation of equations of motion in a nonconservation law form such that stream surfaces form two families of coordinate surfaces. Accurate boundary conditions are applied systematically. Numerical results for a faired wedge, an axisymmetric body and a simple delta wing with sharp supersonic leading edges show that the nonconservation law method has good over-all performance.

Nomenclature

f_β ($\beta = 1,2,3,4$)	= partial derivatives of v^1, α_2, α_3, and p [see Eqs. (6–9)]
$g_{\alpha\beta}$ ($\alpha,\beta = 1,2,3$)	= element of the metric tensor in z-space
J	= Jacobian determinant of the transformation from z-space to x-space
M	= local Mach number
p	= pressure
$q = v^1(g_{11})^{1/2}$	= flow speed
r	= parameter which is zero if x^1, x^2, and x^3 represent Cartesian coordinates and which is unity if x^1, x^2, and x^3 represent cylindrical polar coordinates
$t_\beta{}^\alpha = \partial x^\alpha/\partial z^\beta$	= element of a transformation from z-space to x-space
v^1	= contravariant velocity component
x_L, x_R	= slope of characteristic curves defined in Eq. (11)
x^1, x^2, x^3	= Cartesian or cylindrical polar coordinates
$z^1 = x^1$	= independent variable in the equations of motion
$z^2 = z^2(x^1,x^2,x^3)$	= independent variable and stream function, $z^2 = 0$ on the body surface
$z^3 = z^3(x^1,x^2,x^3)$	= independent variable and stream function
γ	= constant ratio of specific heats
$\Delta z^1, \Delta z^2, \Delta z^3$	= finite-difference mesh sizes
ρ	= density
σ	= a smoothing parameter [see Eq. (23)]
Subscripts	
i,j,k	= indices for position of a mesh point in z-space
∞	= freestream condition

1. Introduction

THIS paper is concerned with a finite-difference method for predicting flowfields generated when a body of given shape moves with steady supersonic speed in air. This is an important practical problem. Designers of supersonic vehicles require accurate information about flow in the neighborhood of the surface of quite complicated body shapes. In particular, predicted values for the surface pressure are needed in order to estimate aerodynamic forces.

Simple finite-difference methods which calculate shock waves automatically without elaborate detection and fitting procedures represent an interesting approach to the problem of computing supersonic flows. Recent work by Kutler and Lomax,[1] and by Kutler, Lomax, and Warming,[2] has done much to demonstrate the promise of the approach. Real shock discontinuities are smoothed but, as results presented in Refs. 1 and 2 show, the computed shock waves remain thin and errors introduced by this particular property of the calculation procedure are usually insignificant.

In the methods of Refs. 1 and 2, at the body surface, reflection boundary conditions or the Abbett[3] procedure, both of which can be programed relatively easily, were used. More accurate procedures based on the theory of characteristics seem to have been rejected because they are regarded as complicated to apply.

The method of this paper was developed for the easy programing of a procedure for applying boundary conditions suggested by the theory of characteristics. Finite-difference representations of characteristic relations are used at a body surface and throughout the flow. The method is of the smooth shock capturing type (SmSC), i.e., shock waves are calculated automatically as thin transition layers across which the dependent variables change rapidly but continuously.

The supersonic flow equations for an inviscid ideal gas with constant specific heats were derived in the form used here by Walkden.[4] The equations and their finite-difference representations are described in Secs. 3 and 4. Two stream functions are used as independent variables, and certain of the equations represent characteristic relations. Consequently, in contrast to other SmSC methods, the finite-difference equations in the present method represent equations of motion in nonconservation law form.

The effectiveness of the method of this paper is assessed by taking numerical results produced by this method and comparing them with theoretical and experimental results that are available for supersonic flows associated with a two-dimensional faired wedge, an axisymmetric waisted body and a delta wing which has supersonic leading edges.

2. Equations of Motion

In the Field

Using the Cartesian tensor summation convention, four of the equations of motion given by Walkden[4] can be expressed in the form

$$e_{\alpha\beta} f_\beta = g_\alpha \quad (\alpha,\beta = 1,2,3,4) \tag{1}$$

where

$$e_{11} = 0.0 \tag{2a}$$

$$e_{12} = -(v^1)^2(x^2)^r t_3{}^3 C_7 \tag{2b}$$

$$e_{13} = (v^1)^2 t_3{}^2 C_7 \tag{2c}$$

$$e_{14} = -x_R(g_{33}x_R + (M)^2 C_2/g_{11})/\rho \tag{2d}$$

Presented at the AIAA Computational Fluid Dynamics Conference, Palm Springs, Calif., July 19–20, 1973; submitted July 30, 1973; revision received December 3, 1973.

* Director, Fluid Mechanics Computation Center.
† Research Assistant, Fluid Mechanics Computation Center.
‡ Scientific Officer, Fluid Mechanics Computation Center.

$$g_1 = -x_R v^1 C_5 C_7/\rho - C_4[x_R(g_{13}x_R+g_{23})-(M)^2C_3/g_{11}]+ C_6[(M)^2C_2/g_{11}+x_R g_{13}]-e_{12}(\partial\alpha_2/\partial z^2)/x_R - e_{13}(\partial\alpha_3/\partial z^2)/x_R - e_{14}(\partial p/\partial z^2)/x_R \quad (2e)$$

$$e_{21} = 0.0 \quad (3a)$$

$$e_{22} = -(v^1)^2(x^2)^r t_3{}^3 C_8 \quad (3b)$$

$$e_{23} = (v^1)^2 t_3{}^2 C_8 \quad (3c)$$

$$e_{24} = -x_L[g_{33}x_L+(M)^2C_2/g_{11}]/\rho \quad (3d)$$

$$g_2 = -x_L v^1 C_5 C_8/\rho - C_4[x_L(g_{13}x_L+g_{23})-(M)^2C_3/g_{11}]+ C_6[(M)^2C_2/g_{11}+x_L g_{33}]-e_{22}(\partial\alpha_2/\partial z^2)/x_L - e_{23}(\partial\alpha_3/\partial z^2)/x_L - e_{24}(\partial p/\partial z^2)/x_L \quad (3e)$$

$$e_{31} = g_{11}v^1 \quad (4a)$$

$$e_{32} = (v^1)^2\alpha_2 \quad (4b)$$

$$e_{33} = (v^1)^2\alpha_3 \quad (4c)$$

$$e_{34} = 1/\rho \quad (4d)$$

$$g_3 = 0.0 \quad (4e)$$

$$e_{41} = g_{13}v^1 \quad (5a)$$

$$e_{42} = (v^1)^2 t_3{}^2 \quad (5b)$$

$$e_{43} = t_3{}^3(x^2)^r(v^1)^2 \quad (5c)$$

$$e_{44} = 0.0 \quad (5d)$$

$$g_4 = -C_4 \quad (5e)$$

$$f_1 = \partial v^1/\partial z^1 \quad (6)$$

$$f_2 = \partial\alpha_2/\partial z^1 \quad (7)$$

$$f_3 = \partial\alpha_3/\partial z^1 \quad (8)$$

$$f_4 = \partial p/\partial z^1 \quad (9)$$

The dependent variables of the problem are p, ρ, v^1, α_2, α_3, x^2, and x^3. The following equations (10–16), determine the right-hand sides of Eqs. (2–5) as functions of the dependent variables and their partial derivatives with respect to z^2 and z^3:

$$C_1 = g_{11}g_{33}-(g_{13})^2 \quad (10a)$$

$$C_2 = g_{12}g_{33}-g_{23}g_{13} \quad (10b)$$

$$C_3 = g_{13}g_{22}-g_{12}g_{23} \quad (10c)$$

$$C_4 = (1/\rho)(\partial p/\partial z^3)+r(v^1)^2\alpha_3(t_1{}^2t_3{}^3-t_3{}^2t_1{}^3) \quad (10d)$$

$$C_5 = -r\rho v^1 t_1{}^2(t_2{}^2t_3{}^3-t_3{}^2t_2{}^3)+\rho v^1(x^2)^r t_2{}^3(\partial\alpha_2/\partial z^3)- \rho v^1 t_2{}^2(\partial\alpha_3/\partial z^3) \quad (10e)$$

$$C_6 = r\alpha_3(v^1)^2(t_1{}^2t_2{}^3-t_2{}^2t_1{}^3) \quad (10f)$$

$$C_7 = [(J)^2+x_R C_2]x_R/J \quad (10g)$$

$$C_8 = [(J)^2+x_L C_2]x_L/J \quad (10h)$$

$$C_9 = (J)^2[1-(M)^2/g_{11}] \quad (10i)$$

$$x_R = \{-C_3-[(C_3)^2-C_9C_1]^{1/2}\}/C_1 \quad (11a)$$

$$x_L = \{-C_3+[(C_3)^2-C_9C_1]^{1/2}\}/C_1 \quad (11b)$$

$$J = (x^2)^r(t_2{}^2t_3{}^3-t_3{}^2t_2{}^3) \quad (12)$$

$$(M)^2 = g_{11}(v^1)^2\rho/\gamma p \quad (13)$$

$$g_{\alpha\beta} = t_\alpha{}^2t_\beta{}^2+(x^2)^{2r}t_\alpha{}^3t_\beta{}^3 \ (\alpha,\beta = 2,3) \quad (14a)$$

$$g_{11} = 1+(\alpha_2)^2+(\alpha_3)^2 \quad (14b)$$

$$g_{12} = \alpha_2 t_2{}^2+\alpha_3(x^2)^r t_2{}^3 \quad (14c)$$

$$g_{13} = \alpha_2 t_3{}^2+\alpha_3(x^2)^r t_3{}^3 \quad (14d)$$

$$\alpha_2 = t_1{}^2 \quad (15a)$$

$$\alpha_3 = (x^2)^r t_1{}^3 \quad (15b)$$

$$t_\beta{}^\alpha = \partial x^\alpha/\partial z^\beta \quad (16a)$$

$$t_1{}^1 = 1.0 \quad (16b)$$

$$t_2{}^1 = 0.0 \quad (16c)$$

$$t_3{}^1 = 0.0 \quad (16d)$$

Since the velocity magnitude is given by

$$(q)^2 = g_{11}(v^1)^2 \quad (17)$$

since the flow is in the direction of the vector

$$(1, \alpha_2, \alpha_3) \quad (18)$$

in x-space, and since the quantities x^2 and x^3 define the transformation from the working z-space to x-space, it follows that the dependent variables provide a complete description of a compressible flow.

Equations obtained by putting $\alpha = 1$ and $\alpha = 2$ in Eq. (1) are characteristic relations which are derived from the equations with independent variables z^1 and z^2 that, in turn, are obtained from the supersonic flow equations when derivatives with respect to z^3 are regarded as quantities which can be represented as functions of the dependent variables through suitable finite difference form approximations. The equations obtained by putting $\alpha = 2$ and $\alpha = 3$ in Eq. (1) express conservation of momentum in the z^1 and z^3 directions, respectively.

The following equations complete the system needed to determine the seven dependent variables:

$$\partial\rho/\partial z^1 = (\rho/\gamma p)\,\partial p/\partial z^1 \quad (19)$$

$$\partial x^2/\partial z^1 = \alpha_2 \quad (20)$$

$$\partial x^3/\partial z^1 = \alpha_3/(x^2)^r \quad (21)$$

At the Body Surface

Equation (1) with $\alpha = 2$ is replaced by the boundary condition

$$\partial\alpha_2/\partial z^1 = \partial^2(x^2)/\partial(z^1)^2$$

It follows that Eqs. (3a–3e) are replaced by

$$e_{21} = 0.0 \quad (22a)$$

$$e_{22} = 1.0 \quad (22b)$$

$$e_{23} = 0.0 \quad (22c)$$

$$e_{24} = 0.0 \quad (22d)$$

and

$$g_2 = \partial^2(x^2)/\partial(z^1)^2 \quad (22e)$$

respectively.

3. Finite-Difference Equations

In the Field

The equations of motion given in Sec. 3 are almost quasi-linear. Thus, when the partial derivatives are replaced by suitable finite-difference expressions, seven algebraic equations relating the dependent variables at the mesh point $(i+1, j, k)$ to variables at the five points $(i, j\pm1, k)$, $(i, j, k\pm1)$ and (i, j, k) are obtained $(j \neq 0)$. These equations are linear in the values of the dependent variables at $(i+1, j, k)$, so the dependent variables at $(i+1, j, k)$ can be calculated easily.

In order to describe the finite-difference equations it is convenient to represent dependent variables at five mesh points by $y(m)$ where m takes integer values from 1 to 35 inclusive. Table 1 relates values of m to mesh points and the dependent variables. For example, it can be seen from Table 1 that $y(5) = (\alpha_3)_{i,j,k-1}$. The notation $(\ )_{i,j,k}$ is used here to denote the value of the quantity inside the bracket at the mesh point (i, j, k).

Now the function $b(n, m)$ with integer arguments n and m is defined to be

$$b(n,m) = (1-\sigma)y(29+n)+0.5\sigma(1-0.5m)A \quad (23a)$$

where

$$A = y(1+n)+y(8+n)+m[y(22+n)+y(15+n)] \quad (23b)$$

Table 1 Integers related to particular dependent variables at given mesh points

Mesh point	p	ρ	v^1	α_2	α_3	x^2	x^3
$(i, j, k-1)$	1	2	3	4	5	6	7
$(i, j, k+1)$	8	9	10	11	12	13	14
$(i, j-1, k)$	15	16	17	18	19	20	21
$(i, j+1, k)$	22	23	24	25	26	27	28
(i, j, k)	29	30	31	32	33	34	35

Then the finite-difference equations for field points ($j \neq 0$) are obtained by making appropriate substitutions in the equations of motion given in Sec. 3. The quantities

$$p = b(0,1) \tag{24a}$$
$$\rho = b(1,1) \tag{24b}$$
$$v^1 = b(2,1) \tag{24c}$$
$$\alpha_2 = b(3,1) \tag{24d}$$
$$\alpha_3 = b(4,1) \tag{24e}$$
$$x^2 = y(34) \tag{24f}$$
$$x^3 = y(35) \tag{24g}$$
$$t_2{}^2 = [y(27)-y(20)]/2\Delta z^2 \tag{25a}$$
$$t_3{}^2 = [y(13)-y(6)]/2\Delta z^3 \tag{25b}$$
$$t_2{}^3 = [y(28)-y(21)]/(2\Delta z^2) \tag{25c}$$
$$t_3{}^3 = [y(14)-y(7)]/(2\Delta z^3) \tag{25d}$$
$$t_1{}^1 = 1.0 \tag{26a}$$
$$t_2{}^1 = 0.0 \tag{26b}$$
$$t_3{}^1 = 0.0 \tag{26c}$$

are subsituted wherever the terms on the left-hand side appear either explicitly or implicitly (e.g., through functions which depend on these terms) in Eqs. (2–5 and 19–21)

$$\partial p/\partial z^3 = [y(8)-y(1)]/(2\Delta z^3) \tag{27a}$$

is substituted in Eq. (10d)

$$\partial \alpha_2/\partial z^3 = [y(11)-y(4)]/(2\Delta z^3) \tag{27b}$$

is substituted in Eq. (10e)

$$\partial \alpha_3/\partial z^3 = [y(12)-y(5)]/(2\Delta z^3) \tag{27c}$$

is substituted in Eq. (10e). The first-order forward difference approximations

$$\partial p/\partial z^2 = [y(22)-b(0,1)]/\Delta z^2 \tag{28a}$$
$$\partial \alpha_2/\partial z^2 = [y(25)-b(3,1)]/\Delta z^2 \tag{28b}$$

and

$$\partial \alpha_3/\partial z^2 = [y(26)-b(4,1)]/\Delta z^2 \tag{28c}$$

are substituted in Eq. (2e).

The first-order backward difference expressions

$$\partial p/\partial z^2 = [b(0,1)-y(15)]/\Delta z^2 \tag{29a}$$
$$\partial \alpha_2/\partial z^2 = [b(3,1)-y(18)]/\Delta z^2 \tag{29b}$$
$$\partial \alpha_3/\partial z^2 = [b(4,1)-y(19)]/\Delta z^2 \tag{29c}$$

are substituted in Eq. (3e). Finally

$$f_4 = \partial p/\partial z^1 = [(p)_{i+1,j,k}-b(0,1)]/\Delta z^1 \tag{30a}$$
$$\partial \rho/\partial z^1 = [(\rho)_{i+1,j,k}-b(1,1)]/\Delta z^1 \tag{30b}$$
$$f_1 = \partial v^1/\partial z^1 = [(v^1)_{i+1,j,k}-b(2,1)]/\Delta z^1 \tag{30c}$$
$$f_2 = \partial \alpha_2/\partial z^1 = [(\alpha_2)_{i+1,j,k}-b(3,1)]/\Delta z^1 \tag{30d}$$
$$f_3 = \partial \alpha_3/\partial z^1 = [(\alpha_3)_{i+1,j,k}-b(4,1)]/\Delta z^1 \tag{30e}$$
$$\partial x^2/\partial z^1 = [(x^2)_{i+1,j,k}-y(34)]/\Delta z^1 \tag{30f}$$

and

$$\partial x^3/\partial z^1 = [(x^3)_{i+1,j,k}-y(35)]/\Delta z^1 \tag{30g}$$

are substituted in Eqs. (1, 19–21). Replacement of partial derivatives with respect to z^2 by forward differences in the right-hand characteristic relation represented by Eq. (1) with $\alpha = 1$, and backward differences in the left-hand characteristic relation (1), with $\alpha = 2$ is a key step which greatly simplifies the task of systematically applying a boundary condition. The procedure was suggested originally by Courant, Isaacson and Rees[5] for problems with two independent variables.

At the Body

On the body surface $z^2 = 0$ and $j = 0$. Points for which $j = -1$ lie inside the body surface where values of the dependent variables are not available. However, by modifying the procedure for constructing algebraic equations from the equations of motion, and by using a finite-difference representation for the boundary condition (22) instead of the left-hand characteristic relation (1), with $\alpha = 2$, the algebraic equations relating the dependent variables at $(i+1, 0, k)$ to dependent variables at the four mesh points $(i, 0, k\pm1)$, $(i, 1, k)$ and $(i, 0, k)$ are obtained. These equations turn out to be linear in the values of the dependent variables at $(i\pm1, 0, k)$ so, these dependent variables can be calculated easily when the shape of the body and the values of the dependent variables at the points $(i, 0, k\pm1)$, $(i, 1, k)$ and $(i, 0, k)$ are all known.

Now a brief description will be given of both the way in which the finite-difference representation of Eq. (22e) is constructed and the changes that have to be made in the construction of algebraic representations of the equations of motion.

$$(x^3)_{i+1,0,k} = (x^3)_{i,0,k}+\Delta z^1 y(33)/[y(34)]^r \tag{31}$$

and

$$(x^1)_{i+1,0,k} = (z^1)_{i+1,0,k} \tag{32}$$

Thus, if the body shape is described so that x^2 is a known function of x^1 and x^3, then the right-hand side of Eq. (22e) can be approximated by

$$[(x^2)_{i+1,0,k}-2(x^2)_{i,0,k}+(x^2)_{i-1,0,k}]/(\Delta z^1)^2 \tag{33}$$

where

$$(x^2)_{i+1,0,k} = x^2[(x^1)_{i+1,0,k}, (x^3)_{i+1,0,k}] \tag{34}$$

is calculated from the given equation for the body shape. The quantities $(x^2)_{i,0,k}$ and $(x^2)_{i-1,0,k}$ can be regarded as known.

If it is remembered that Eq. (1) with $\alpha = 2$ is replaced by the boundary condition defined by Eq. (22), the procedure for constructing algebraic representations of the equations of motion and boundary condition at the body surface is the same as that described for field points provided the following modifications are made to certain of the equations given earlier:

1) Replace the quantities $b(n, 1)$ for $n = 0, 1, 2, 4$ in Eqs. (24a–24e, 28, and 30a–30e) by $b(n, 0)$. Replace $b(3, 1)$ in Eq. (24d) by $y(32)$. *Note* the function $b(n, m)$ is defined by Eq. (23).

2) Replace Eqs. (25a) and (25c) by

$$t_2{}^2 = [y(27)-y(34)]/\Delta z^2 \tag{35a}$$

and

$$t_2{}^3 = [y(28)-y(35)]/\Delta z^2 \tag{35b}$$

The modifications outlined in paragraphs 1 and 2 are needed to avoid calling values of the dependent variables at mesh points inside the body.

Numerical Stability

Due to the way in which the finite-difference equations have been constructed, a theoretical stability analysis cannot be completed readily. For the present investigation, numerical stability trials were carried out. These trials suggest that the method outlined here is conditionally stable provided $\sigma \neq 0$. The numerical experiments do not yield an explicit stability criterion. It can be stated only that, provided $\sigma \neq 0$, stable

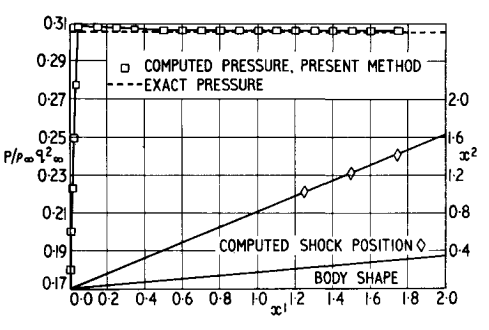

Fig. 1 Surface pressure distribution and shock shape for faired wedge at $M = 2.0$.

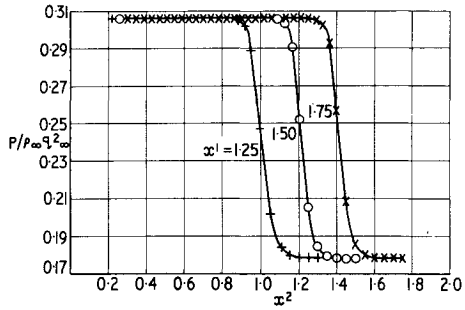

Fig. 2 Pressure distributions normal to the uniform stream for faired wedge at $M = 2.0$.

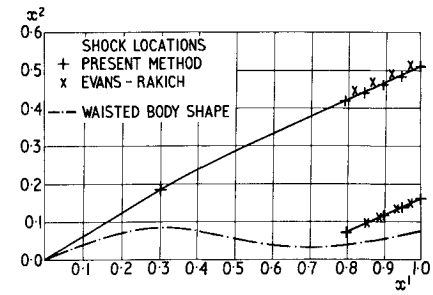

Fig. 3 Waisted body and computed shock shapes.

numerical results can generally be obtained by making Δz^1 small enough.

4. Faired Wedge

Body Shape

The supersonic flow around a faired wedge placed at zero incidence in a uniform stream has been calculated. The problem has been solved by calculating the flow past a wall described by the equations

$$x^2 = 0 \qquad x^1 < 0.0 \tag{36a}$$

$$x^2 = 1.76327(x^1)^2 \qquad 0.0 \leqq x^1 \leqq 0.05 \tag{36b}$$

$$x^2 = 0.176327(x^1) - 0.004408175 \qquad x^1 > 0.05 \tag{36c}$$

This problem was studied in order to assess whether or not a computational procedure based on the finite-difference equations given in this paper can capture shock waves satisfactorily. The wall shape for $x^1 > 0$ is plotted in Fig. 1. In this case $r = 0$, so x^1 and x^2 are Cartesian coordinates.

Numerical Results

Flow at a Mach number of 2 has been calculated for the case when $\sigma = 0.1$, $\Delta z^1 = 0.001$, and $\Delta z^2 = 0.01$ so that the fairing is covered by 50 mesh points. Starting with uniform flow at $z^1 = x^1 = 0$, 1750 integration steps have been taken in the z^1-direction. The computer program was arranged so that the flow was computed only at points where it was disturbed from uniform stream values. Outside the disturbed region, $z^2 = x^2$ because the streamlines are parallel to the x^1-axis. The equations of motion have been made nondimensional so that $\rho_\infty = 1$, $q_\infty = 1$, and $p_\infty = 1/\gamma(M_\infty)^2$.

Some numerical results are plotted in Figs. 1 and 2. The dotted line representing "the exact solution" is, in fact, the solution for flow at $M_\infty = 2$ past an unfaired wedge defined by the equation

$$x^2 = 0.176327x^1 \tag{37}$$

Thus, the dotted line represents the asymptotic value of the pressure which the numerical solution ought to approach as $x^1 \to \infty$, $z^1 \to 0$, and $z^2 \to 0$. The diamond shapes in Fig. 1 indicate the shape of the computed shock wave. The continuous line through the diamonds is the shape of the shock wave associated with flow at $M_\infty = 2$ past the unfaired wedge (37). As expected, at large distances from the corner, the computed shock wave has the same slope as the shock wave associated with the unfaired wedge. For a given value of $x^1 = i\Delta z^1$, the computed shock wave has been located at

$$x^2 = 0.5[(x^2)_{i,n} + (x^2)_{i,n+1}]$$

where n is an integer such that

$$|(p_{i,n+1} - p_{i,n})/[(x^2)_{i,n+1} - (x^2)_{i,n}]|$$

is a maximum. If the dependent variables at mesh points $(i\Delta z^1, j\Delta z^2)$ for $0 \leqq j \leqq N$ are different from their uniform stream values, then n will have a value between 0 and N.

Figure 2 shows the variation of pressure with x^2 for three constant values of x^1. The extent to which the shock discontinuity is smoothed on account of large truncation error effects in the neighborhood of the shock can be seen in this figure. Clearly, the smoothing effects diminish with distance from the shock wave. In the present case, at $x^1 = 1.25$, over 85% of the shock layer region between the body and the true bow shock wave, the truncation error is less than 10% of the pressure jump through the shock. At $x^1 = 1.75$ the error is less than 10% over 90% of the shock layer region. The computed shock wave may be regarded as having thickness equal to 15% of the thickness of the shock layer region between the wedge and the bow shock wave at $x^1 = 1.25$. Similarly, at $x^1 = 1.75$, the thickness of the computed shock is 10% of the shock layer thickness.

5. Axisymmetric Waisted Body

Body Shape

The supersonic flow surrounding a waisted body with shape defined by five equations of the form

$$x^2 = a_0 + a_1(x^1) + a_2(x^1)^2 + a_3(x^1)^3 + a_4(x^1)^4 \tag{38}$$

for $(x^1)_0 \leqq x^1 \leqq (x^1)_1$ has been calculated.

Values for $(x^1)_0$, $(x^1)_1$ and the coefficients a_n, $n = 0, 1, 2, 3, 4$, are given in Table 2.

The shape of the waisted body is shown in Fig. 3. It can be seen from Table 2 that the nose of the body is conical for

$$0 \leqq x^1 \leqq 0.14158$$

In this case the parameter $r = 1$ so that x^2 represents distance from the axis in a cylindrical polar coordinate system.

Table 2 Coefficients describing the shape of a waisted body[a]

Segment	$(x^1)_0$	$(x^1)_1$	a_0	a_1	a_2	a_3	a_4
1	0.0	0.14158	0.0	0.363970	0.0	0.0	0.0
2	0.14158	0.45725	−0.00461	0.334980	1.226680	−6.492210	6.34730
3	0.45725	0.64473	0.229694	−0.595521	0.607620	−0.236382	0.0
4	0.64473	0.76317	−12.4939	72.96859	−158.03866	150.87806	−53.58258
5	0.76317	1.0	−0.064001	0.290242	−0.390789	0.236382	0.0

[a] $x^2 = a_0 + a_1(x^1) + a_2(x^1)^2 + a_3(x^1)^3 + a_4(x^1)^4$ for $(x^1)_0 \leqq x^1 \leqq (x^1)_1$.

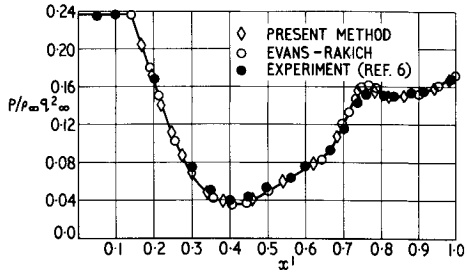

Fig. 4 Comparison of surface pressures for a waisted body at $M = 2.793$

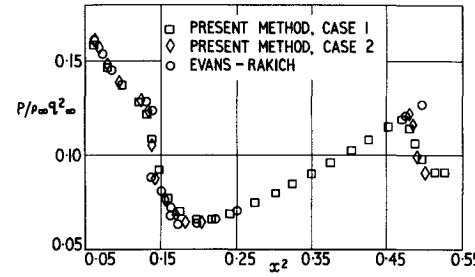

Fig. 6 Comparison of pressure distributions normal to the uniform stream for a waisted body at $M = 2.793$, $x^1 = 0.95$.

Numerical Results

Starting from the known axisymmetric cone solution at

$$z^1 = x^1 = 0.14158 \tag{39}$$

the flow at a Mach number of 2.793 has been calculated in two cases with different mesh sizes

case 1: $\Delta z^1 = 0.001$ $\Delta z^2 = 0.00216153$

case 2: $\Delta z^1 = 0.0004$ $\Delta z^2 = 0.00072051$

The value $\sigma = 0.1$ was used in both case 1 and case 2. Some numerical results are plotted in Figs. 3–6.

Figure 3 shows computed shapes of both the bow shock and an internal shock. The criterion outlined in the third paragraph of Sec. 5 was used to locate the shock positions plotted in this figure.

Figure 4 is a graph of the pressure distribution on the body surface. The surface pressures calculated by the present method in case 2 are compared with experimental results given by Winter, Rotta, and Smith,[6] and with numerical results obtained by Evans,[7] who employed a modified form of a computer program based on the method of characteristics as described by Inouye, Rakich and Lomax.[8]

Figures 5 and 6 show the distribution of pressure with distance from the axis for two constant values of x^1. In Fig. 5, $x^1 = 0.3$ and in Fig. 6, $x^1 = 0.95$. It can be seen from Figs. 4–6 that the results obtained using the method of this paper are in good agreement with those obtained by Evans using the method of characteristics. The extent to which shock discontinuities are smoothed because of large truncation error effects in the immediate neighborhood of a discontinuity can be seen in Figs. 5 and 6. Of course, the smoothing decreases with distance from a shock wave. In the present example, for the bow shock wave, with the coarse mesh (case 1), at $x^1 = 0.3$, the truncation error is less than 10% of the pressure jump through the shock wave over 92% of the shock layer. At $x^1 = 0.95$ the error is less than 10% over 95% of the shock layer region. The computed shock thickness may be defined as 8% of the thickness of the shock layer region between the body surface and the bow shock at $x^1 = 0.3$, and 5% at $x^1 = 0.95$. For the fine mesh (case 2) the computed shock thickness is smaller. At both $x^1 = 0.3$ and $x^1 = 0.95$, using the criterion that the computed shock occupies a region within which truncation errors in the pressure are greater than 10% of the pressure jump through the shock wave, the computed shock thicknesses are only 3% of the thickness of the shock layer.

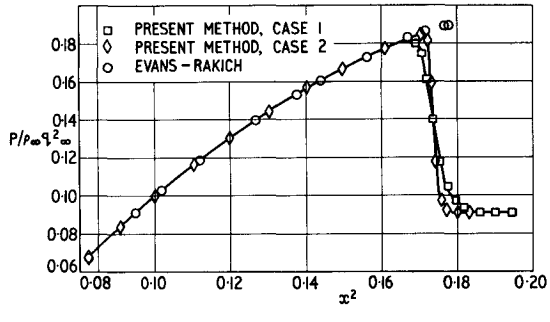

Fig. 5 Comparison of pressure distributions normal to the uniform stream for a waisted body at $M = 2.793$, $x^1 = 0.3$.

The bow shock wave is located in slightly different positions by the two methods (see Figs. 5 and 6). The difference between the predicted positions for the bow show increases with x^1. The differences range from about 1% at $x^1 = 0.3$ to about 2% at $x^1 = 0.95$. The exact shock location is not known, but the shock position predicted by the method of characteristics program used by Evans appears to be in error at $x^1 = 0.3$ where, although the pressure behind the shock and, therefore, the shock slope are both less than corresponding values for the nose cone, the predicted shock position lies on the line representing the conical shock associated with the nose cone.

6. Delta Wing

Wing Shape

Flow over the upper surface and flow over the lower surface of a delta wing defined by the following equations have been calculated for a case when the wing leading edges are supersonic

$$x^2 = a_0 + a_1(x^1 - \alpha) + a_2(x^1 - \alpha)^2 + a_3(x^1 - \alpha)^3 \tag{40a}$$

for

$$\alpha \leqq x^1 \leqq \alpha + \varepsilon \tag{40b}$$

where

$$\alpha = |x^3| \tan\beta / \tan\theta - 0.5\varepsilon \tag{40c}$$

for

$$-\infty \leqq x^3 \leqq \infty \tag{40d}$$

$$x^2 = -x^1 \tan\theta \tag{40e}$$

for

$$\alpha + \varepsilon < x^1 \tag{40f}$$

where α is given by Eq. (40c)

$$\tan\beta = \sin\theta / \tan\lambda \tag{40g}$$

The wing defined by Eqs. (40) has a delta planform and zero thickness. The shape may be described as a plane delta wing with leading edges that are drooped so that in a uniform stream parallel to the x^1-axis the slope $(\partial x^2/\partial x^1)$ of the wing is zero at the leading edge. As x^1 increases the slope decreases steadily to a constant value of $-\tan\theta$ for all values of x^3 and values of x^1 defined by Eq. (40f). The constant value $-\tan\theta$ is attained at a distance ε from the leading edge. The quantity λ in Eq. (40g) is the sweepback angle.

For this example, the parameter r in the equations of Secs. 3 and 4 is chosen equal to zero so that x^1, x^2, and x^3 are coordinates in a Cartesian system.

Numerical Results

Computations have been carried out for a wing described by Eqs. (40) with

$$\theta = 4° \tag{41a}$$

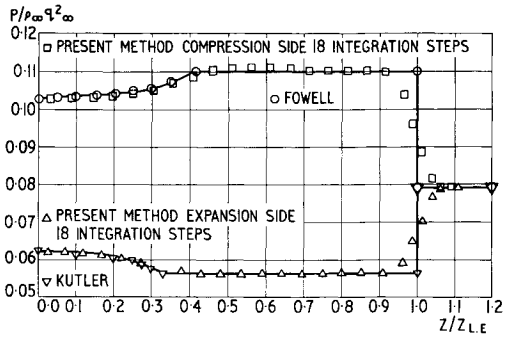

Fig. 7 Comparisons of spanwise surface pressure distributions for the expansion and compression sides of a delta wing.

$$\lambda = 45^\circ \tag{41b}$$

and

$$\varepsilon = 0.05$$

For the computations the wing was placed in a uniform stream of Mach number 3. The uniform stream flow direction was parallel to the x^1-axis. With this flow Mach number, the wing leading edges are supersonic, and the flows over the upper and lower surfaces of the wing do not interfere with each other and therefore they can be computed separately.

At large distances from the leading edge, the solution for the wing described by Eqs. (40) can be expected to approach the solution for a plane delta wing of zero thickness with sweepback angle of 45° placed at incidence in a uniform stream with $M_\infty = 3$.

The plane delta wing problem for the upper surface has been considered by Kutler and Lomax[1] and the corresponding lower surface problem has been considered by Fowell.[9]

Starting with the uniform flow solution in the plane $x^1 = 0$, flow over the upper surface and over the lower surfaces of the wing described by Eqs. (40) with constants given by Eqs. (41) has been calculated in the case where

$$\Delta z^1 = 0.03 \tag{42a}$$

$$\Delta z^2 = 0.05 \tag{42b}$$

$$\Delta z^3 = 0.05 \tag{42c}$$

$$\sigma = 0.25 \tag{43}$$

The computer program was arranged so that the flow was computed only at points where it was disturbed from uniform stream values. The dependent variables were made nondimensional so that $\rho_\infty = 1$, $q_\infty = 1$, and $p_\infty = 1/\gamma(M_\infty)^2$.

In the neighborhood of the wing surface, the basic finite-difference mesh defined by Eqs. (42) was subdivided by a factor 4.

Some numerical results that have been obtained using the method of this paper are shown in Fig. 7. In this figure spanwise distributions of surface pressures on the upper and lower surfaces of the wing are compared with results obtained by other workers. For the expansion side, the comparison is with Kutler and Lomax's[1] results. For the compression side, the comparison is with results given by Fowell.[9] As expected, in both cases, agreement is good except in the immediate neighborhood of the wing leading edge.

In Fig. 7

$$z/z_{\text{L.E}} = x^3/(x^3)_{\text{L.E}} \tag{44}$$

where for a given value of x^1

$$(x^3)_{\text{L.E}} = x^1 \tan\theta/\tan\beta \tag{45}$$

All the numerical results obtained using the finite-difference equations described in the present paper have been obtained using an ICL KDF9 computer [KDF9 speed = (1/60)× CDC7600 speed, KDF9 core store = 26K words for program and data].

7. Conclusions

In view of the numerical results that have been obtained using the method of this paper, it is concluded that the shock capturing numerical method based on finite-difference equations constructed from the equations of motion in Sec. 3 is an appropriate method for calculating arbitrary supersonic three-dimensional flowfields. In particular, the procedure for applying boundary conditions is satisfactory and satisfactory computed shock waves are produced by the method.

Individual equations of motion upon which the method of this paper is based are not in conservation law form, therefore, it is also concluded that having equations of motion in conservation law form is not necessary in order to produce computed shock waves which propagate through a flowfield correctly.

References

[1] Kutler, P. and Lomax, H., "A Systematic Development of the Supersonic Flowfields over and behind Wings and Wing-Body Configurations Using a Shock-Capturing Finite-Difference Approach," *Journal of Spacecraft and Rockets,* Vol. 8, No. 12, Dec. 1971, pp. 1175–1182.

[2] Kutler, P., Lomax, H., and Warming, R. F., "Computation of Space Shuttle Flowfields Using Noncentered Finite-Difference Schemes," *AIAA Journal,* Vol. 11, No. 2, Feb. 1973, pp. 196–204.

[3] Abbett, M. J., "Boundary Condition Computational Procedures for Inviscid Supersonic Steady Flow Field Calculations," Final Rept. 71-41, 1971, Aerotherm Corp., Mt. View, Calif.

[4] Walkden, F., "A Form of the Supersonic Flow Equations for an Ideal Gas," ARC Rept. 34160, 1972, British Aeronautical Research Council, London, England (unpublished).

[5] Courant, R., Isaacson, E., and Rees, M., "On the Solution of Nonlinear Hyperbolic Differential Equations by Finite Differences," *Communications in Pure and Applied Mathematics,* Vol. 5, 1952, pp. 243–255.

[6] Winter, K. G., Rotta, J. C., and Smith, K. G., "Studies of the Turbulent Boundary Layer on a Waisted Body of Revolution in Subsonic and Supersonic Flow," TR 68215, 1968, Royal Aircraft Establishment, Farnborough, England.

[7] Evans, D., private communication, Nov. 1972, Univ. of Salford, Salford, England.

[8] Inouye, M., Rakich, J. V., and Lomax, H., "A Description of Numerical Methods and Computer Programs for Two Dimensional and Axisymmetric Supersonic Flow over Blunt-Nosed and Flared Bodies," TN D-2970, 1965, NASA.

[9] Fowell, L. R., "Exact and Approximate Solutions for the Supersonic Delta Wing," *Journal of the Aeronautical Sciences,* Vol. 23, 1956, p. 709.